Ultracompact Low-Threshold Organic Laser

Parag B. Deotare,*,† Thomas S. Mahony,† and Vladimir Bulović

Massachusetts Institute of Technology, 77 Massachusetts Avenue, Cambridge, Massachusetts 02139, United States. †These authors contributed equally.

ABSTRACT We report an ultracompact low-threshold laser with an Alq_3:DCM host:guest molecular organic thin film gain layer. The device uses a photonic crystal nanobeam cavity which provides a high quality factor to mode volume (Q/V) ratio and increased spontaneous emission factor along with a small footprint. Lasing is observed with a threshold of 4.2 $\mu J/cm^2$ when pumped by femtosecond pulses of $\lambda = 400$ nm wavelength light. We also model the dynamics of the laser and show good agreement with the experimental data. The inherent waveguide geometry of the structure enables easy on-chip integration with potential applications in biochemical sensing, inertial sensors, and data communication.

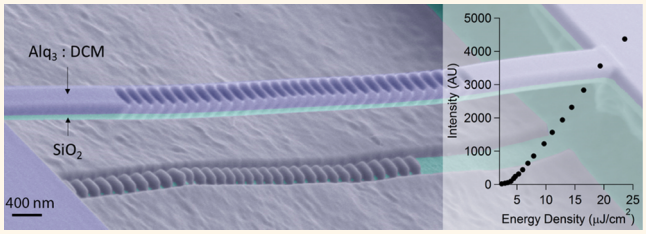

KEYWORDS: photonic crystal · nanobeam cavities · nanolasers · organic laser dye · Alq_3:DCM

The demonstration of strong absorption and high-efficiency emission from semiconducting organic films has renewed interest in solid-state dye lasers.[1] Organic lasers are particularly suitable for tunable operations due to the broad gain spectrum of dye molecules.[2] These lasers are known for delivering high pulse energies with narrow bandwidth. Study of enhanced light emission and decay rates of organic dyes coupled to various microcavity structures such as micropillars,[3] 2D photonic crystals,[4,5] and 1D photonic crystals[6] has been reported in the literature. Lasing has been reported under photoexcitation in devices with distributed Bragg reflectors,[7−11] distributed feedback structures,[12−14] whispering gallery resonators,[15] photonic band gap fiber resonators,[16] and 2D photonic crystals.[17−20] However, no demonstration of an electrically pumped organic laser has yet been reported. The major limiting factor is attributed to singlet−triplet annihilation leading to infeasible threshold current densities.[21,22] A possible way to tackle this problem is to lower the threshold by controlling the device optical properties, such as quality factor/mode volume (Q/V) and/or spontaneous emission factor (β), which in this work we attempt by using a photonic crystal nanobeam cavity (PCNC).[23]

We report compact, waveguide integratable, low-threshold organic lasers based on tris(8-hydroxyquinolinato)aluminum (Alq_3) film doped with 4-(dicyanomethylene)-2-methyl-6-(4-dimethylaminostyryl)-4*H*-pyran laser dye, forming an Alq_3:DCM host:guest system containing 2.5 wt % of DCM molecules. To the best of our knowledge, this is the smallest footprint organic laser to be reported. Photonic crystal nanobeam cavities that provide very high Q/V and allow for easy on-chip integration due to their waveguide geometry are fabricated using the organic films. Such structures are also known to have a high β which further helps in reducing the threshold of the laser.[24] The β refers to the fraction of spontaneous emission that is coupled into the lasing mode. Since the local density of optical states in a PCNC is limited by the photonic band gap (in one dimension), β approaches unity for such devices, a value that is between 2 and 4 orders of magnitude higher than for a DBR microcavity structure. It has been shown before that optical excitation of Alq_3:DCM films leads to lasing action.[1,10] Alq_3 molecules are pumped to the excited state with a $\lambda = 400$ nm wavelength excitation laser pulse. The exited molecule transfers the energy to a nearby DCM molecule through Förster resonant energy transfer (FRET). The FRET process in a host:guest system enables efficient excitation of DCM molecules, as the light is primarily absorbed by the Alq_3 molecules that then efficiently transfer their exciton energy to the fewer dispersed DCM guest molecules.

* Address correspondence to pdeotare@mit.edu.

Received for review August 8, 2014 and accepted September 17, 2014.

Published online September 22, 2014
10.1021/nn504444g

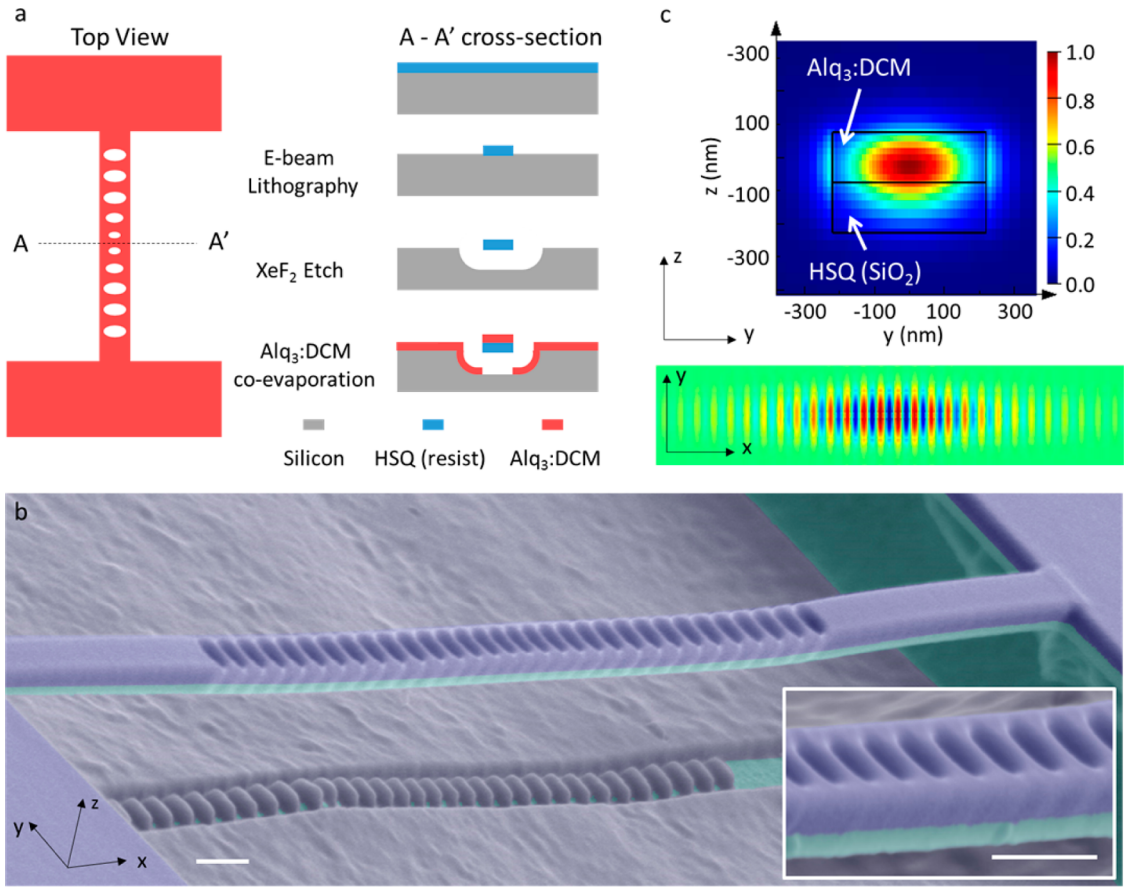

Figure 1. Photonic crystal nanobeam cavity. (a) Schematic of the cross section along the AA′ axis for different steps of the fabrication process. (b) SEM image of a fabricated device. Scale bars in the figure and the inset correspond to 400 nm. (c) Simulated electric field along the cross section of the structure showing the field confinement in the gain medium and the simulated electric field (E_y) profile of the cavity mode.

We use a bottom-up approach for fabricating the nanopatterned devices since conventional electron-beam lithography and reactive ion etching techniques can damage the molecular organic films. The suspended mask patterns are fabricated on silicon substrates using the electron-beam lithography (Elionix, 125 kV) with XR-1541-4 (hydrogen silsesquioxane (HSQ)) negative electron-beam resist followed by XeF_2 etch (Figure 1a). The samples are transferred into a vacuum chamber (10^{-6} Torr base pressure), where a 150 nm thick layer of Alq_3:DCM is then coevaporated onto the suspended PCNCs. Avoiding exposure to the atmosphere, the samples are transferred from the vacuum chamber into a nitrogen glovebox, where they are packaged using a nonsolvent epoxy (Torrseal). A SEM image of an unpackaged PCNC structure is shown in Figure 1b. Comparing the SEM image to that prior to evaporation revealed that the nanobeams buckled during the evaporation process. Inset also shows sidewall roughness and angled growth of the evaporated films.

The nanobeam cavities were designed using commercially available finite difference time domain software (Lumerical Solutions, Inc.) following the design guidelines outlined in earlier work.[23] The width and thickness of each layer were selected to maintain structural integrity of the waveguide, limit the number of modes, and maintain high field overlap with the organic layer. The width of the nanobeam was set to 440 nm, and the thickness of the HSQ and organic layer was set to be 150 nm each. The cross section of the device plotted in Figure 1c shows the high mode confinement inside the organic material. This enables design of a hybrid structure where the cavity is formed using the gain medium.[25,26] A periodicity of 270 nm for the elliptical holes, with major and minor diameters of 300 and 130 nm, respectively, generated a band gap centered at λ = 610 nm wavelength, which corresponded to the peak of emission of the Alq_3:DCM film. The cavity was formed by tapering the six central holes forming the fundamental cavity mode resonance at λ = 627 nm. The number of mirror holes, flanking the tapered holes, was limited to 10 to achieve a modest Q. The electric field profile (E_y) of the fundamental mode is also shown in Figure 1c. Cavities with Q values over a million were designed by increasing the number of tapered and mirror holes even though the index of refraction of the Alq_3:DCM films is relatively low, n = 1.7. However, the roughness of the evaporated film was a limiting factor for the Q, and hence all the experiments were done on devices designed with a Q = 10 000.

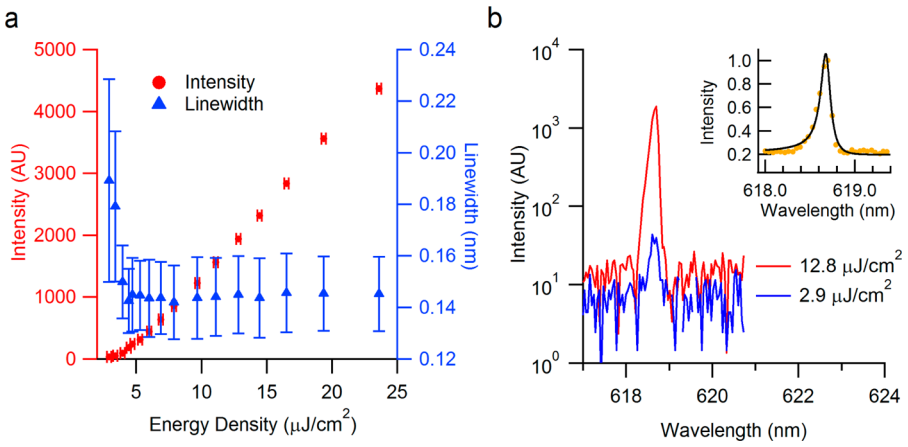

Figure 2. (a) Red filled circles denote the output intensity of the optical mode for various absorbed input pulse energy densities. Blue triangles show the corresponding linewidth of the mode. Linewidth narrowing at the threshold is observed as a confirmation for lasing. (b) Output spectrum of device below (blue line) and above (red line) the threshold. For easy comparison, the background emission from the spectrum at 600 nm has been subtracted. Inset shows the Fano line shape fit to the spectrum used to extract the linewidth.

RESULTS AND DISCUSSION

Figure 2 shows a plot of the output intensity of the fundamental cavity mode for various pump energy densities. A laser threshold is observed at an absorbed input pulse energy density of 4.2 μJ/cm^2. The sudden narrowing of the emission linewidth at the threshold pump energy confirmed lasing behavior. The emission spectrum from the device below and above the threshold is plotted in Figure 2b. Lasing was observed through the fundamental mode of the cavity at λ = 618.5 nm. The discrepancy (~1.3%) between the designed and fabricated device wavelength is attributed to imperfections during the fabrication process. The inset shows spectral data fitted to a Fano line shape[27] to extract the linewidth (refer to the Methods section).

Lasing in the current system can be modeled using the following rate equations:[28]

$$\frac{dN_{Alq_3}}{dt} = \tilde{F} - \frac{N_{Alq_3}(t)}{\tau_{Alq_3}} - \frac{N_{Alq_3}(t)}{\tau_{FRET}} \quad (1)$$

$$\frac{dN_{DCM}}{dt} = \frac{N_{Alq_3}(t)}{\tau_{FRET}} - \frac{F_m v_g \sigma_{se} N_{DCM}(t)}{V_m} - \frac{F_s v_g \sigma_{se} N_{DCM}(t)}{V_m} - \frac{N_{DCM}(t)}{\tau_{DCM,nr,PC}} - v_g \sigma_{se} N_{DCM}(t) N_p(t) \quad (2)$$

$$\frac{dN_p(t)}{dt} = \Gamma v_g \sigma_{se} N_{DCM}(t) N_p(t) + \frac{\Gamma F_m v_g \sigma_{se} N_{DCM}(t)}{V_m} - \frac{N_p(t)}{\tau_{cav}} \quad (3)$$

N_{Alq_3} and N_{DCM} represent the excited state density (LUMO) of Alq_3 and DCM, respectively, while N_p represents the photon density of the lasing mode. Equation 1 describes the dynamics of the Alq_3 molecules. $\tilde{F}$ is the input photon density flux (m^{-3} s^{-1}), which was estimated using $\eta(E_{in})/(\hbar\omega_p\delta_{duty}t_{act})$, where E_{in} is the pump energy density per excitation pulse, η is the fraction of energy absorbed by the film, ω_p is the pump frequency, δ_{duty} is the duty cycle of the excitation pulses, and t_{act} is the active layer thickness. The last two terms represent the loss mechanism due to radiative and nonradiative decay (τ_{Alq_3} = 16 ns) and FRET (τ_{FRET} = 10 ps) to DCM molecules.

Equation 2 describes the population dynamics of the DCM molecules. The first term denotes the rate at which the DCM excitons are created due to FRET. The second term refers to the rate of loss of excitons that are coupled to the cavity mode due to radiative decay. F_m is the Purcell factor which gives the amount by which the radiative lifetime of DCM is reduced due to the presence of the microcavity. The next term represents the radiative decay into the radiation modes followed by a term representing the total nonradiative loss of the system. The last term accounts for the stimulated photons; σ_{se} (1×10^{-16} cm^2) is the stimulated emission cross section of DCM, and v_g and V_m represent the group velocity and mode volume of the lasing mode, respectively.

Equation 3 describes the dynamics for photons in the lasing mode. The first term represents the rate density at which cavity mode photons are created by stimulated emission followed by a term representing the spontaneous emission photons into the lasing mode. Γ is the power confinement factor which was calculated using FDTD simulations to be 0.5 for the fundamental mode. The last term represents the loss of photons due to leakage from the cavity, which depends on the cavity lifetime ($\tau_{cav} = Q/\omega$). The Q for the tested device was measured to be 3600. With the current representation of the laser, the spontaneous emission factor is given by $\beta = F_m/(F_m + F_s)$, where F_s represents the change in radiation lifetime of uncoupled DCM molecules to the microcavity.

We pump the system using ultrafast laser pulses of ~100 fs long, which can be treated as δ functions. Transient measurements of DCM molecules show a reduction in lifetime from 2.9 ns in bulk to 2.6 ns in the

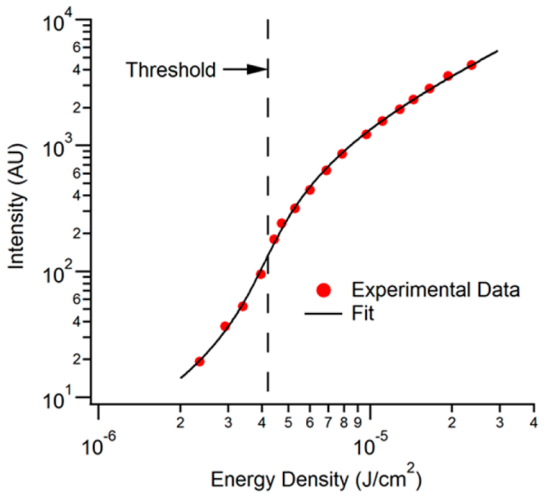

Figure 3. Log−log plot of the experimental intensity data. The solid line is the numerical fit to the data.

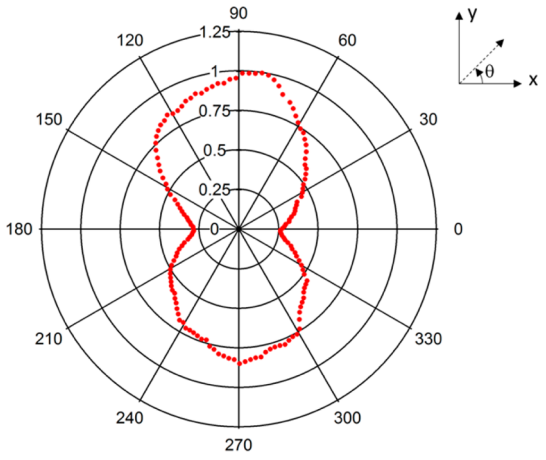

Figure 4. Polarization measurements showing the dipole emission profile of the device.

photonic crystal. We expect that this reduction is mostly dominated by nonradiative loss due to the increase in surface area in the photonic crystal. We assume a DCM radiative lifetime of 5 ns and fit the data shown in Figure 2a to give β and F_m of 0.017 and 2.6, respectively. This value of β is 2 orders of magnitude larger when compared to the distributed Bragg reflector-based devices[28] yet smaller compared to values reported in the literature for similar structures, primarily due to the low index of refraction of the organic material that results in weaker confinement. Figure 3 shows the experimental intensity data on log−log axes, showing the saturation of the output power at high pump intensities. The solid line is the fitted curve that shows very good agreement with the experimental data. The dotted line marks the threshold above which superlinear increase of emission with pump power corresponding to lasing is observed. The log−log plot also reveals that the threshold of the laser is much softer due to higher value of β.

Figure 4 shows the far-field emission profile of the device taken at a constant input power above the threshold. The dipole pattern resembles the characteristic emission from the fundamental mode of the PCNC. It should be noted that the devices were engineered such that the cavity loss was dominated by out-of-plane scattering to help with the measurement. For on-chip applications, the devices can be designed to emit along the waveguide.

CONCLUSION

In conclusion, we demonstrated the first low-threshold organic laser in a photonic crystal nanobeam cavity geometry. This structure enables high Q/V as well as a high spontaneous emission factor, which are both important in reducing the laser threshold. The quality factor of these devices is limited by the roughness of the patterned and deposited films. Improving the surface roughness will improve the Q and further lower the threshold, advancing organic laser designs toward the desired demonstration of an electrically pumped organic laser. These lasers are the smallest organic lasers to be reported, and their waveguide geometry enables potential use in on-chip communication. The suspended structure makes these devices suitable to be used in optomechanical applications such as highly sensitive motion sensors.[29,30] Finally, the current geometry allows the gain material to be directly accessible to the environment and hence can be used as amplifying biochemical sensors where the photophysical properties of the organic lasing gain medium are altered by the addition of impurities.[14] In such structures, the adsorption of molecules on the cavity surface introduces additional nonradiative pathways for recombination, altering the lasing behavior and allowing for high sensitivity chemosensing.

METHODS

Mask Fabrication. The mask patterns are fabricated on silicon substrates using electron-beam lithography (Elionix, 125 kV) with the XR-1541-4 (HSQ) negative electron-beam resist. The samples are developed using 25% aqueous tetramethylammoniumhydroxide for 14 s followed by a thorough rinse in DI water. Etching the underlying silicon substrate with XeF_2 gas leads to free-standing HSQ structures.

Coevaporation of Organic Films. Organic films are deposited onto the substrate by thermal evaporation in a vacuum of $\sim 3 \times 10^{-6}$ to 8×10^{-7} Torr. The thickness of the materials is continuously monitored using a pair of crystal quartz monitors. Each monitor is first calibrated by depositing 50 nm of material onto a bare silicon substrate and measuring the thickness of the film using a J.A. Woollam variable angle spectroscopic ellipsometer (VASE). Postcalibration, Alq_3 and DCM are coevaporated onto the patterned substrate. The 2.5% DCM concentration of the final film is achieved by evaporating Alq_3 at an average rate that is 40 times faster than DCM. After evaporation, the substrates are transferred through vacuum to a nitrogen-filled glovebox, where they are sealed between two glass coverslips using vacuum epoxy (Torrseal).

Optical Characterization of Devices. The devices are probed using 100 fs long excitation pulses centered at $\lambda = 400$ nm, which are generated at 1 kHz using a mode-locked regeneratively amplified laser system that pumped an optical parametric amplifier. The excitation light beam is expanded, and the center of the beam is focused to an 11 μm diameter spot on the device surface through a 50$\times$ objective to achieve a uniform excitation density in the device active layer. The emitted light is collected using the same objective lens, spectrally filtered using a dichroic and band-pass filter to remove any residue of the pump laser light, and coupled to a multimode fiber before being analyzed on a spectrometer (Princeton Instruments, Inc.). The intensity of the pump laser is varied using a variable neutral density filter. Polarization measurements are performed by placing a thin film polarizer mounted on a motorized rotation stage in the output path before the collection fiber of the spectrometer.

Transient Measurements. Time-correlated single-photon counting technique is carried out using a single-photon detecting avalanche photodiode (APD) (MPD PDM series 50 μm). The output of the APD is connected to a timing module with a resolution of 4 ps (PicoQuant PicoHarp 300). Lifetime measurements of DCM molecules showing a reduction in lifetime due to photonic crystal structure are carried out by illuminating the mirror section of the nanobeams.

Linewidth Extraction. The spectral data are fitted with a Fano line shape[27] given by

$$F(\lambda) = A_0 + F_0 \frac{[q+2(\lambda - \lambda_0)/\gamma]^2}{1+[2(\lambda - \lambda_0)/\gamma]^2}$$

where λ_0 is the wavelength of the resonance mode, γ is the resonance linewidth, A_0 and F_0 are constants, and q is the asymmetric factor which accounts for the ratio between resonant and nonresonant amplitudes.

Conflict of Interest: The authors declare no competing financial interest.

Acknowledgment. Financial support was provided by the Department of Energy, Basic Energy Sciences, Energy Frontiers Research Center for Excitonics and the National Science Foundation (Award No. 1001994). TM acknowledges support from National Science Graduate Research Fellowship (Grant No. 1122374). Device fabrication was performed in part at the Center of Nanoscale Systems at Harvard and MIT's Microsystems Technology Laboratories. Measurements were performed in the MIT Nanostructured Materials Metrology Laboratory within the MIT Center for Materials Science and Engineering on equipment provided by the ENI-MIT Solar Frontiers Center.

REFERENCES AND NOTES

1. Kozlov, V. G.; Bulovic, V.; Burrows, P. E.; Forrest, S. R. Laser Action in Organic Semiconductor Waveguide and. *Nature* **1997**, *389*, 362–364.
2. Schneider, D.; Rabe, T.; Riedl, T.; Dobbertin, T.; Kröger, M.; Becker, E.; Johannes, H.-H.; Kowalsky, W.; Weimann, T.; Wang, J.; *et al.* Ultrawide Tuning Range in Doped Organic Solid-State Lasers. *Appl. Phys. Lett.* **2004**, *85*, 1886.
3. Adawi, A. M.; Lidzey, D. G. Enhancing the Radiative Decay Rate of Fluorescent Organic Molecules Using Micropillar Microcavities and Optical Nanocavities. *Mater. Sci. Eng., B* **2008**, *149*, 266–269.
4. Adawi, A. M.; Murshidy, M. M.; Fry, P. W.; Lidzey, D. G. An Optical Nanocavity Incorporating a Fluorescent Organic Dye Having a High Quality Factor. *ACS Nano* **2010**, *4*, 3039–3044.
5. Kitamura, M.; Iwamoto, S.; Arakawa, Y. Enhanced Light Emission from an Organic Photonic Crystal with a Nanocavity. *Appl. Phys. Lett.* **2005**, *87*, 151119.
6. Murshidy, M. M.; Adawi, A. M.; Fry, P. W.; Lidzey, D. G. A One-Dimensional Photonic-Crystal Nanocavity Incorporating a Fluorescent Molecular Dye. *Appl. Phys. Lett.* **2010**, *97*, 153303.
7. Akselrod, G. M.; Young, E. R.; Bradley, M. S.; Bulović, V. Lasing through a Strongly-Coupled Mode by Intra-cavity Pumping. *Opt. Express* **2013**, *21*, 12122.
8. Berggren, M.; Dodabalapur, A.; Slusher, R. E. Stimulated Emission and Lasing in Dye-Doped Organic Thin Films with Forster Transfer. *Appl. Phys. Lett.* **1997**, *71*, 2230.
9. Kéna-Cohen, S.; Forrest, S. Room-Temperature Polariton Lasing in an Organic Single-Crystal Microcavity. *Nat. Photonics* **2010**, *4*, 371–375.
10. Bulović, V.; Kozlov, V. G.; Khalfin, V. B.; Forrest, S. R. Transform-Limited, Narrow-Linewidth Lasing Action in Organic Semiconductor Microcavities. *Science* **1998**, *279*, 553–555.
11. Yoon, J.; Lee, W.; Caruge, J.-M.; Bawendi, M.; Thomas, E. L.; Kooi, S.; Prasad, P. N. Defect-Mode Mirrorless Lasing in Dye-Doped Organic/Inorganic Hybrid One-Dimensional Photonic Crystal. *Appl. Phys. Lett.* **2006**, *88*, 091102.
12. Kowalsky, W.; Rabe, T.; Schneider, D.; Johannes, H.-H.; Karnutsch, C.; Gerken, M.; Lemmer, U.; Wang, J.; Weimann, T.; Hinze, P.; *et al.* Organic Semiconductor Distributed Feedback Laser. In *Nanosensing: Materials and Devices II* (Proceedings of SPIE); Islam, M. S., Dutta, A. K., Eds.; SPIE Publications: Cardiff, U.K., 2005; Vol. 6008, pp 60080Z-15.
13. Schneider, D.; Rabe, T.; Riedl, T.; Dobbertin, T.; Kröger, M.; Becker, E.; Johannes, H.-H.; Kowalsky, W.; Weimann, T.; Wang, J.; *et al.* Laser Threshold Reduction in an All-Spiro Guest–Host System. *Appl. Phys. Lett.* **2004**, *85*, 1659.
14. Rose, A.; Zhu, Z.; Madigan, C. F.; Swager, T. M.; Bulovic, V. Sensitivity Gains in Chemosensing by Lasing Action in Organic Polymers. *Nature* **2005**, *434*, 876–879.
15. Vietze, U.; Krauß, O.; Laeri, F.; Ihlein, G.; Schüth, F.; Limburg, B.; Abraham, M. Zeolite–Dye Microlasers. *Phys. Rev. Lett.* **1998**, *81*, 4628–4631.
16. Shapira, O.; Kuriki, K.; Orf, N. D.; Abouraddy, A. F.; Benoit, G.; Viens, J. F.; Rodriguez, A.; Ibanescu, M.; Joannopoulos, J. D.; Fink, Y.; *et al.* Surface-Emitting Fiber Lasers. *Opt. Express* **2006**, *14*, 3929–3935.
17. Gourdon, F.; Chakaroun, M.; Fabre, N.; Solard, J.; Cambril, E.; Yacomotti, A.-M.; Bouchoule, S.; Fischer, A.; Boudrioua, A. Optically Pumped Lasing from Organic Two-Dimensional Planar Photonic Crystal Microcavity. *Appl. Phys. Lett.* **2012**, *100*, 213304.
18. Meier, M.; Mekis, A.; Dodabalapur, A.; Timko, A.; Slusher, R. E.; Joannopoulos, J. D.; Nalamasu, O. Laser Action from Two-Dimensional Distributed Feedback in Photonic Crystals. *Appl. Phys. Lett.* **1999**, *74*, 7.
19. Mekis, A.; Meier, M.; Dodabalapur, A.; Slusher, R. E.; Joannopoulos, J. D. Rapid Communication Lasing Mechanism in Two-Dimensional Photonic Crystal Lasers. *Appl. Phys. A: Mater. Sci. Process.* **1999**, *114*, 111–114.
20. Riechel, S.; Kallinger, C.; Lemmer, U.; Feldmann, J.; Gombert, A.; Wittwer, V.; Scherf, U. A Nearly Diffraction Limited Surface Emitting Conjugated Polymer Laser Utilizing a Two-Dimensional Photonic Band Structure. *Appl. Phys. Lett.* **2000**, *77*, 2310.
21. Baldo, M.; Holmes, R.; Forrest, S. Prospects for Electrically Pumped Organic Lasers. *Phys. Rev. B* **2002**, *66*, 035321.
22. Giebink, N.; Forrest, S. Temporal Response of Optically Pumped Organic Semiconductor Lasers and Its Implication for Reaching Threshold under Electrical Excitation. *Phys. Rev. B* **2009**, *79*, 073302.
23. Deotare, P. B.; McCutcheon, M. W.; Frank, I. W.; Khan, M.; Lončar, M. High Quality Factor Photonic Crystal Nanobeam Cavities. *Appl. Phys. Lett.* **2009**, *94*, 121106.
24. Zhang, Y.; Khan, M.; Huang, Y.; Ryou, J.; Deotare, P.; Dupuis, R.; Lončar, M. Photonic Crystal Nanobeam Lasers. *Appl. Phys. Lett.* **2010**, *97*, 051104.
25. Barrelet, C. J.; Bao, J.; Loncar, M.; Park, H.-G.; Capasso, F.; Lieber, C. M. Hybrid Single-Nanowire Photonic Crystal and Microresonator Structures. *Nano Lett.* **2006**, *6*, 11–15.
26. Yang, Q.; Jiang, X.; Guo, X.; Chen, Y.; Tong, L. Hybrid Structure Laser Based on Semiconductor Nanowires and a Silica Microfiber Knot Cavity. *Appl. Phys. Lett.* **2009**, *94*, 101108.
27. Galli, M.; Portalupi, S. L.; Belotti, M.; Andreani, L. C.; O'Faolain, L.; Krauss, T. F. Light Scattering and Fano Resonances in High-*Q* Photonic Crystal Nanocavities. *Appl. Phys. Lett.* **2009**, *94*, 071101.

28. Koschorreck, M.; Gehlhaar, R.; Lyssenko, V. G.; Swoboda, M.; Hoffmann, M.; Leo, K. Dynamics of a High-*Q* Vertical-Cavity Organic Laser. *Appl. Phys. Lett.* **2005**, *87*, 181108.
29. Krause, A.; Winger, M.; Blasius, T.; Lin, Q.; Painter, O. A High-Resolution Microchip Optomechanical Accelerometer. *Nat. Photonics* **2012**, *6*, 768–772.
30. Deotare, P. B.; Bulu, I.; Frank, I. W.; Quan, Q.; Zhang, Y.; Ilic, R.; Loncar, M. All Optical Reconfiguration of Optomechanical Filters. *Nature Comm.* **2012**, *3*, 846.